SCIENTIFIC REVIEW

Probing cosmology beyond ΛCDM using SKA

SHAMIK GHOSH[1,2], PANKAJ JAIN[3], RAHUL KOTHARI[4,*] , MOHIT PANWAR[3],
GURMEET SINGH[3] and PRABHAKAR TIWARI[5]

[1]CAS Key Laboratory for Researches in Galaxies and Cosmology, Department of Astronomy, University of Science and Technology of China, Chinese Academy of Sciences, Hefei 230026, Anhui, People's Republic of China.

[2]School of Astronomy and Space Science, University of Science and Technology of China, Hefei 230026, People's Republic of China.

[3]Department of Physics, Indian Institute of Technology, Kanpur 208016, India.

[4]Department of Physics and Astronomy, University of the Western Cape, Cape Town 7535, South Africa.

[5]National Astronomical Observatories, Chinese Academy of Science, Beijing 100101, People's Republic of China.

*Corresponding author. E-mail: quantummechanicskothari@gmail.com

Abstract.   The cosmological principle states that the Universe is statistically homogeneous and isotropic at large distance scales. Currently, there exist many observations which indicate a departure from this principle. It has been shown that many of these observations can be explained by invoking superhorizon cosmological perturbations and may be consistent with the Big Bang paradigm. Remarkably, these modes simultaneously explain the observed Hubble tension, i.e., the discrepancy between the direct and indirect measurements of the Hubble parameter. We propose several tests of the cosmological principle using SKA. In particular, we can reliably extract the signal of dipole anisotropy in the distribution of radio galaxies. The superhorizon perturbations also predict a significant redshift dependence of the dipole signal, which can be well tested by the study of signals of reionization and the dark ages using SKA. We also propose to study the alignment of radio galaxy axes as well as their integrated polarization vectors over distance scales ranging from a few Mpc to Gpc. We discuss data analysis techniques that can reliably extract these signals from data.

Keywords.   Cosmological principle—superhorizon perturbations—square kilometre array.

1. Introduction

Current observations support an expanding universe. If we extrapolate this back in time, we can infer that the Universe started from a very hot and dense state. This event, known as Big Bang, marked the origin of the Universe in a very high temperature state.

To make the problem of expansion dynamics tractable, we assume that the Universe is spatially isotropic and homogeneous. This assumption is also known as Cosmological Principle (CP) (Einstein 1917; Kolb & Turner 1994; Aluri *et al.* 2022). It turns out that Hubble's law is a direct consequence of CP (Coles & Lucchin 2003). Furthermore, it can be shown that the most general spacetime metric that describes the universe following CP is the FLRW metric (Weinberg 1972; Coles & Lucchin 2003). It is also important to mention that CP is an independent assumption and does not follow from symmetries of the Einstein's equations.

The FLRW metric describes the Universe with a smooth background having an exact isotropic and homogeneous matter distribution. But observationally, the Universe also possesses structure in the form of stars, galaxies, etc. These structures arise due to the curvature perturbations, which are seeded during the epoch of exponential expansion called inflation. The resulting cosmological model, including dark matter and dark energy is called ΛCDM.

Although, these perturbations are not isotropic and homogeneous per se, they satisfy these properties in a statistical sense. For example, in the cosmic frame of rest, the matter density is expected to be the same at all points provided we average over a sufficiently large distance scale. The precise value of this distance scale is still not clear, but is expected to be of order 100 Mpc (see e.g., Kim *et al.* 2021).

It has been speculated that during an epoch, before inflation ensued, the Universe may be described by a complicated metric, whose nature is currently poorly understood. However, it quickly evolves to the isotropic and homogeneous FLRW metric during inflation, perhaps within the first e-fold. Wald (1983) for the first time, gave an explicit demonstration for Bianchi Universes. Some other results also exist for inhomogeneous metric (Jensen & Stein-Schabes 1986; Stein-Schabes 1987). We may speculate that the idea generalizes to a larger class of metrics.[1] The Big Bang paradigm is therefore consistent with an early anisotropic and/or inhomogeneous phase of the Universe. Given the existence of such a phase, it is clearly important to ask whether it has any observational consequences.

Observationally, the Universe is found to be consistent with CP to a good approximation. But currently, there exist many observations in CMB and large scale structures (LSS) which appear to violate CP (Ghosh *et al.* 2016). We review these anomalies later in Section 2. For an expansive review, see Aluri *et al.* (2022). There exist many theoretical attempts to explain these observations. It has been suggested that superhorizon modes, i.e., perturbations of wavelengths larger than the horizon size (Grishchuk & Zeldovich 1978a, b), may explain some of these observations (Gordon *et al.* 2005; Erickcek *et al.* 2008a, b; Ghosh 2014; Das *et al.* 2021; Tiwari *et al.* 2022). Additionally, these can account for low-ℓ alignments (Gao 2011), though these can not extenuate the present accelerated expansion of the Universe (Flanagan 2005; Hirata & Seljak 2005). It is assumed that such large wavelength modes are aligned with one another and hence do not obey CP. An intriguing possibility is that such modes might originate during an anisotropic and/or inhomogeneous pre-inflationary phase of the Universe (Aluri & Jain 2012; Rath *et al.* 2013). Hence, despite being in violation with CP, they would be consistent with the Big Bang paradigm.
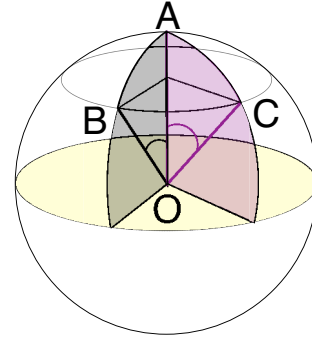
Figure 1. Illustration of statistical isotropy. In this figure, A, B and C are given points on the spherical surface such that $\angle AOB = \angle AOC$.

1.1 *Mathematical formulation and ramifications*

To relate theory with observations, we seek ensemble averages of the fields under consideration. Ergodicity hypothesis (Ellis *et al.* 2012) allows us to relate this ensemble averaging to the space averaging. It is known that for the Gaussian random fields, all the statistical information is contained in the two point correlation functions (2PCF). However, in the presence of non-Gaussianities, we need higher order correlators like bispectrum (3PCF) or trispectrum (4PCF), etc., to extract optimal cosmological information. CP dictates that the nPCF only be a function of distances between the points $\mathbf{x}_i \equiv (z_i, \mathbf{n}_i)$. Thus:

$$\langle \rho(\mathbf{x}_1)\rho(\mathbf{x}_2) \ldots \rho(\mathbf{x}_n) \rangle = f(x_{12}, x_{13}, \ldots, x_{ij}, \ldots),$$
(1)

where $x_{ij} = |\mathbf{x}_i - \mathbf{x}_j| = x_{ji}$ and $i \neq j$. Clearly, this makes this nPCF invariant under arbitrary translations and rotations. The condition (1) for 2PCF in case of a 2D field, e.g., CMB temperature, takes the usual form

$$\langle T(\mathbf{x}_1)T(\mathbf{x}_2) \rangle \equiv \langle T(\hat{\mathbf{m}})T(\hat{\mathbf{n}}) \rangle = f(\hat{\mathbf{m}} \cdot \hat{\mathbf{n}}),$$
(2)

with $\mathbf{x}_1 \equiv (z_*, \hat{\mathbf{n}})$ and $\mathbf{x}_2 \equiv (z_*, \hat{\mathbf{m}})$, z_* being the redshift to decoupling. Equation (2) is the familiar result for the 2PCF, which dictates that the temperature correlation depends only upon the angle between the locations. This is illustrated in Figure 1, where three points A, B and C are chosen in a manner such that $\angle AOC = \angle AOB$. Thus, we must have $\langle T(\mathbf{A})T(\mathbf{C}) \rangle = \langle T(\mathbf{A})T(\mathbf{B}) \rangle$, since $\mathbf{A} \cdot \mathbf{C} = \mathbf{A} \cdot \mathbf{B}$.

2. Observations at tension with ΛCDM

Our observations in the past two decades have firmly planted the inflationary ΛCDM cosmology as the standard paradigm. A vast set of observables from CMB to

---

[1]There are exceptions to these results as well (Sato 1988).

LSS broadly agree with ΛCDM predictions. Despite the successes of ΛCDM, we have a growing set of observations that are at tension with our expectations from ΛCDM. We will summarize some of the observed tensions, in the context of the model discussed in this paper. See Perivolaropoulos & Skara (2022) for a review.

2.1 Observed violations of statistical isotropy

As we discussed before, CP implies statistical isotropy and homogeneity. Due to our fixed vantage point, it is not possible to directly test statistical homogeneity. However, we can test statistical isotropy. Various observational tests, performed on different cosmological datasets, amply attest statistical isotropy violations. Some of these are reviewed in Ghosh *et al.* (2016).

2.1.1 Kinematic dipole As explained in the Section 1, CP is valid only in the cosmic frame of rest. We as observers are not stationary with respect to this frame on account of the motion of Earth, the Sun, and the Milky Way. This gives rise to an effective peculiar velocity to our observation frame. This peculiar velocity results in a Doppler boost of the CMB temperature fluctuation, further culminating in a kinematic dipole in the CMB temperature fluctuations. Interpreting the CMB dipole to be of kinematic origin (Planck Collaboration *et al.* 2014) leads to the peculiar velocity of our local frame to be 384 ± 78 km s^{-1}.

The peculiar velocity **v** of our observation is expected to give rise to a dipole in the observed number count of sources. The local motion would cause a Doppler and aberration effects, both of which contribute to a dipole in the observed number counts (Ellis & Baldwin 1984). For sources with flux, following a power law relation in frequency: $S \propto \nu^{-\alpha}$, and with differential number count $N(S, \hat{\mathbf{n}}) = S^{-1-x}$, the expected dipole is given by:

$$\mathbf{D} = [2 + x(1 + \alpha)]\mathbf{v}/c, \tag{3}$$

where c is the speed of light, α is the frequency scaling spectral index and $(1 + x)$ is the slope of $\ln N$ v/s $-\ln S$ plot. We can use the estimates of our peculiar velocity from the CMB and use it to predict the estimated dipole in the large-scale structure data. Assuming $\alpha \approx 0.75$ and $x \approx 1$, we found the expected dipole $D_{\text{th}} \sim 0.005$. Measurements of the dipole in LSS surveys at $z \sim 1$ have yielded results that are consistent with CMB direction, but the magnitude is found to be double or more of the predicted value. In Table 1, we list the measured value of dipole in the

Table 1. Results for the dipole in LSS exceed the expected value of 5×10^{-3}.

Authors	$|\mathbf{D}|$ $(\times 10^{-2})$	(l, b)
Singal (2011)	1.8 ± 0.3	$(239°, 44°)$
Rubart & Schwarz (2013)	1.6 ± 0.6	$(241°, 39°)$
Tiwari *et al.* (2015)	1.25 ± 0.40	$(261°, 37°)$
Tiwari & Nusser (2016)	0.9 ± 0.4	$(246°, 38°)$
Colin *et al.* (2017)	1.6 ± 0.2	$(241°, 28°)$
Secrest *et al.* (2021)	1.5	$(238°, 29°)$

NVSS, NVSS+WENSS, NVSS+SUMSS and CatWISE catalogs. The dipole measured in the LSS has a much larger magnitude than expected from CMB measurements, but is consistent with the CMB dipole direction. The deviation is found to be at 4.9σ in the CatWISE data (Secrest *et al.* 2021).

We pointed out that the assumed power law dependence of number counts on S is not strictly valid (Tiwari *et al.* 2015). This leads to a difference in the dipole in number counts and in sky brightness. It also introduces a dipole in the mean flux per source. Hence, this provides a non-trivial test of whether the dipole is indeed of kinematic origin. This idea has been generalized in Nadolny *et al.* (2021), who develop a method to extract kinematic dipole independently from an intrinsic dipole.

2.1.2 Alignment of quadrupole ($\ell = 2$) and octupole ($\ell = 3$) Both $\ell = 2, 3$ CMB multipoles are aligned with preferred direction pointing roughly along the CMB dipole (de Oliveira-Costa *et al.* 2004). Physically, both of these multipoles form a planar structure, such that the perpendicular to this plane is aligned with the CMB dipole.

2.1.3 Alignment of galaxy axes and polarizations There have been many observations, both in optical (Hutsemékers 1998) and radio (Tiwari & Jain 2013; Taylor & Jagannathan 2016) data sets that suggest alignment of galaxy axes and integrated linear polarizations. These observations can be nicely explained in terms of the correlated magnetic field, which may be of primordial origin (Tiwari & Jain 2016). Intriguingly, the optical alignment is seen to be very prominent in the direction of the CMB dipole (Ralston & Jain 2004).

2.1.4 Dipole in radio polarization offset angles The integrated polarizations of radio galaxies are known to be aligned approximately perpendicular to the galaxy position axes. Remarkably, the angle between these two

axes shows a dipole pattern in the sky with preferred axis again pointing roughly along the CMB dipole (Jain & Ralston 1999). Hence, we see that several diverse observations appear to indicate the same preferred direction. Taken together, they are strongly suggestive of a violation of the CP (Ralston & Jain 2004).

2.1.5 Dipole modulation and the hemispherical asymmetry   We found that the CMB temperature fluctuations have slightly higher power in the southern ecliptic hemisphere than the northern one. This is called the hemispherical power asymmetry and was first observed in the WMAP data (Hoftuft *et al.* 2009) and continues to persist in the Planck measurements (Planck Collaboration *et al.* 2020). It is also observed that the CMB temperature fluctuations appear to be modulated by a dipole that points close to the south ecliptic pole. This implies that the CMB temperature fluctuation along line-of-sight direction $\hat{\mathbf{n}}$ is given by:

$$\Delta T(\hat{\mathbf{n}}) = \Delta T_{\mathrm{iso}}[1 + A\hat{\lambda} \cdot \hat{\mathbf{n}}], \tag{4}$$

where ΔT_{iso} satisfies CP, A is the amplitude of the dipole and $\hat{\lambda}$ is the preferred direction. Current Planck measurements (Planck Collaboration *et al.* 2020) give $A = 0.070^{+0.032}_{-0.015}$ and $\hat{\lambda} = (221°, -21°) \pm 31°$. Such a dipole modulation would lead to difference in powers in the two hemispheres along $\hat{\lambda}$.

2.1.6 Other CMB observations   Other observations of SI violations in the CMB are low in significance, albeit they are present in both WMAP and Planck data. For low-ℓ values, the even multipoles are anomalously smaller than the odd multipole modes in power. This is called the parity asymmetry. The largest asymmetry are evidenced in the lowest multipoles, viz., $\ell \in [2, 7]$. These low multipoles show an anomalously small power, which is called the low power on large scales in the CMB temperature fluctuations.

2.2 *Hubble tension*

Hubble tension is the disagreement in measured value of the Hubble parameter H_0 from different methods. The local universe measurements of H_0 using the 'distance ladder' method with Cepheids and supernovae type Ia (SNIa) or strong lensing systems differ from the measurements from the CMB assuming ΛCDM. Other methods like tip of the red giant branch (TRGB) (Reid *et al.* 2019) or gravitational wave events (Gayathri *et al.* 2020; Mukherjee *et al.* 2020) have measured value nearly between the two. Broadly speaking, H_0 measurements from the local universe is larger than

the measurements from the CMB at nearly 5σ significance (Anchordoqui & Perez Bergliaffa 2019). It has been suggested that the Hubble tension may lead to a breakdown of FLRW metric based cosmology (see Krishnan *et al.* 2021 for more details).

The Cepheid–SNIa measurements use Cepheid variables in host galaxies of SNIa, to calibrate the distance. These calibrated type Ia supernovae are then used to calibrate magnitude and redshift of a large sample of SNIa. The full sample of SNIa probes the Hubble flow and is used to directly infer the Hubble parameter. Riess *et al.* (2019) estimate the value $H_0 = 74.03 \pm 1.42$ km s^{-1} Mpc^{-1}. This agrees with the Freedman *et al.* (2012) estimate of $H_0 = 74.3 \pm 2.1$ km s^{-1} Mpc^{-1}. The H0LiCOW team's (Wong *et al.* 2020) recent measurement, using the time delay for a system of six gravitationally lensed quasars, yields $H_0 = 73.3^{+1.7}_{-1.8}$ km s^{-1} Mpc^{-1} that agrees very well with Cepheid (Freedman *et al.* 2001) measurements.

In addition to the aforementioned 'direct' measurements, CMB can also be used to infer the value of the Hubble parameter 'indirectly'. The CMB T and E mode measurements are used to fit the ΛCDM model. In its basic form, ΛCDM has only six parameters. The Hubble parameter can be estimated indirectly from the best fit. This indirect estimation of the H_0 gives a value lower than the direct measurements. Planck Collaboration *et al.* (2018) gives $H_0 = 67.27 \pm 0.60$ km s^{-1} Mpc^{-1} using only T and E mode data. Estimates of H_0 using other CMB experiments like ACT (Dunkley *et al.* 2011) and SPTpol (for $\ell < 1000$) (Henning *et al.* 2018) give consistent results with Planck.

3. Superhorizon perturbation model

It has been suggested that the superhorizon perturbations can explain the observed violations of statistical isotropy. These are perturbations with wavelengths larger than the particle horizon (Erickcek *et al.* 2008a). Such modes necessarily exist in a cosmological model. However, to explain the observed violations of isotropy (Gordon *et al.* 2005), we also need them to be aligned with one another. In Gordon *et al.* (2005), such an alignment is attributed to a stochastic phenomenon known as spontaneous breakdown of isotropy. Alternatively, the alignment may be attributed to an intrinsic violation of the cosmological principle. A very interesting possibility is presented in Aluri & Jain (2012) and Rath *et al.* (2013). It is argued that during its very early phase, the Universe may not be isotropic and homogeneous. As

Table 2. Some parameter values for the superhorizon mode (Equation 5) explaining NVSS excess dipole and also resolving the Hubble tension. These values are also satisfying CMB constraints that are taken from Tiwari *et al.* (2022).

	ω	ϱ	κ/H_0
1	0.81π	0.97	2.58×10^{-3}
2	0.81π	0.48	6.4×10^{-3}

explained in Section 1, it acquires this property during inflation (Wald 1983). The modes which originate during the early phase of inflation when the Universe deviates from isotropy and homogeneity may not obey the cosmological principle (Rath *et al.* 2013). We postulate that these are the aligned superhorizon modes.

3.1 *Resolution of various anomalies*

Cosmological implications of this phenomenon have been obtained by assuming the existence of a single adiabatic mode (Erickcek *et al.* 2008a, b; Ghosh 2014; Das *et al.* 2021; Tiwari *et al.* 2022). Working in the conformal Newtonian gauge, such a mode can be expressed as:

$$\Psi_p = \varrho \sin(\kappa x_3 + \omega). \tag{5}$$

Thus, a superhorizon mode is characterized by its amplitude ϱ, wavenumber κ and phase factor $\omega \neq 0$. In Equation (5), we have taken the mode to be aligned along the x_3 (or z) axis, which we also assume to be the direction of CMB dipole. For a superhorizon mode, we have $\kappa/H_0 \ll 1$.

It has been shown that such a superhorizon mode is consistent with all existing cosmological observations (like CMB, NVSS constraints, etc.) for a range of parameters (Ghosh 2014; Das *et al.* 2021; Tiwari *et al.* 2022). Some parameter values are given in Table 2. It can affect the large scale distribution of matter and can potentially explain the enigmatic excess dipole signal observed in the radio galaxy distribution (Singal 2011; Gibelyou & Huterer 2012; Rubart & Schwarz 2013; Tiwari *et al.* 2015; Tiwari & Jain 2015; Tiwari & Nusser 2016; Colin *et al.* 2017).

The observed matter dipole, D_{obs} is expressed as:

$$\mathbf{D}_{obs} = (D_{kin} + D_{grav} + D_{int})\hat{x}_3, \tag{6}$$

where D_{kin}, D_{grav} and D_{int}, respectively, denote the amplitudes of the kinematic, gravitational and intrinsic dipoles. These components are redshift-dependent. Thus, we can write the magnitude of the observed dipole

between the redshifts z_1 and z_2, due to the superhorizon mode (5) as

$$D_{obs}(z_1, z_2) = [\mathscr{A}_1(z_1, z_2) + \mathscr{A}_2(z_1, z_2) + \mathscr{C}(z_1, z_2)]$$
$$\times \frac{\varrho\kappa\cos\omega}{H_0} + \mathscr{B}, \tag{7}$$

where the term:

$$\mathscr{B} = [2 + x(1+\alpha)]\frac{v}{c}, \tag{8}$$

is the redshift-independent kinematic dipole component. The explicit expressions for other redshift-dependent factors $\mathscr{A}_1(z_1, z_2)$, $\mathscr{A}_2(z_1, z_2)$, $\mathscr{C}(z_1, z_2)$ are given in Das *et al.* (2021). Notice that in the absence of a superhorizon mode, i.e., $\varrho \rightarrow 0$, the dipole magnitude in Equation (7), as expected, becomes redshift-independent and equal to (3).

3.1.1 Matter dipole Due to the presence of an aligned superhorizon mode, an additional contribution to our velocity arises with respect to LSS in the CMB dipole direction. This is given in Equation (2.12) of Das *et al.* (2021). Hence, it leads to a change in D_{kin} in comparison to its prediction based on CMB dipole (Das *et al.* 2021). Furthermore, the superhorizon mode contributes through the Sachs-Wolfe (SW) and the integrated Sachs-Wolfe (ISW) effects (Erickcek *et al.* 2008a), thereby leading to D_{grav} in Equation (6). Finally, the superhorizon mode leads to an intrinsic anisotropy in the matter distribution and hence contributes to D_{int}. Equation (7) is the explicit expression considering all these effects. From the equation, it is clear that for a given value of $\varrho > 0$, the dipole contribution is maximum if $\omega = \pi$. All the contributions due to the mode depend on redshift since the mode has a systematic dependence on distance and hence, the predicted dipole is redshift-dependent.

It is interesting to note that the contributions of the superhorizon mode to the CMB dipole, cancel out at the leading order (Erickcek *et al.* 2008a). Such a cancellation does not happen in the case of matter dipole (Das *et al.* 2021). We may understand this as follows. As per Equation (6), there are three different contributions to the matter dipole—(a) the kinematic dipole which arises due to our velocity relative to the source, (b) the gravitational dipole (SW and ISW) and (c) the intrinsic dipole. In the case of CMB, these three add up to zero. In the case of matter dipole, the kinematic dipole explicitly depends on the parameter α, which arises in the spectral dependence of the flux from a source, as well as the parameter x (Equation 8), which arises in the number count distribution. Furthermore, the gravitational effect also depends on α. The intrinsic dipole,

however, does not depend on either of these parameters. We point out that both these parameters arise at non-linear order in the theory of structure formation and furthermore the assumed power law distribution is only an approximation (Tiwari *et al.* 2015). These parameters are best extracted from observations and cannot be reliably deduced theoretically. Hence, the situation is very different in the case of matter dipole in comparison to CMB dipole and we do not expect that the two would behave in the same manner. We clarify that in the case of matter dipole, the superhorizon perturbation is treated at first order in perturbation theory. However, the small wavelength modes, which are responsible for structure formation have to be treated at nonlinear order. In Das *et al.* (2021), the existence of structures is assumed as given with their properties deduced observationally and the calculation focuses only on the additional contribution due to the superhorizon mode. However, a complete first principles calculation would have to treat small wavelength modes at nonlinear order.

There are some further issues (see Domènech *et al.* 2022 for more details), associated with gauge invariance (Challinor & Lewis 2011; Bonvin & Durrer 2011), which are not addressed in Das *et al.* (2021). These issues are very important, but to the best of our understanding, they are expected to lead to small corrections to the calculational framework used in Das *et al.* (2021) and not expected to qualitatively change their results. It will be very interesting to repeat these calculations using the gauge invariant framework, but this is beyond the scope of the present paper. Such a calculation must also take into account the fact that the aligned superhorizon modes, we are considering do not arise within the ΛCDM model, but perhaps due to an anisotropic/inhomogeneous early phase of cosmic expansion (Aluri & Jain 2012; Rath *et al.* 2013).

3.1.2 Alignment of quadrupole and octupole   Further, the superhorizon mode can also explain the alignment of CMB quadrupole and octupole (Gordon *et al.* 2005). With x_3 axis along the CMB dipole, it leads to non-zero spherical harmonic coefficients T_{10}, T_{20}, T_{30} in the temperature anisotropy field (Erickcek *et al.* 2008a). We obtain constraints on the mode parameters in Equation (5) by necessiating that T_{20} and T_{30} are less than three times the measured rms values of the quadrupole and octupole powers, respectively (Erickcek *et al.* 2008a). It turns out that the dipole contribution does not lead to a significant constraint. These contributions can explain the alignment of quadrupole and octupole if we assume the presence of an intrinsic contribution to T_{10} and T_{20}, which is partially cancelled by the contribution due to

the superhorizon mode. Note that this intrinsic contribution is statistical in nature and hence, its exact value cannot be predicted.

3.1.3 Hubble tension   It has been shown by Das *et al.* (2021) that a superhorizon mode leads to a perturbation in the gravitational potential between distant galaxies and us. This culminates in a correction in observed redshift of galaxies

$$1 + z_{\mathrm{obs}} = (1 + z)(1 + z_{\mathrm{Doppler}})(1 + z_{\mathrm{grav}}). \tag{9}$$

Thus, we see that in the presence of superhorizon modes, the galaxy at redshift z is observed instead at a redshift z_{obs}. In the above equation, the redshifts z_{Doppler} and z_{grav} are, respectively, due to our velocity relative to LSS and perturbation in potential introduced by the superhorizon mode. We can express z_{obs} as (Das *et al.* 2021; Tiwari *et al.* 2022):

$$z_{\mathrm{obs}} = \bar{z} + \gamma \cos\theta + \cdots , \tag{10}$$

where the first and second terms on the RHS are the monopole and dipole terms. Here, θ is the polar angle of the source with x_3 axis along the CMB dipole and γ the dipole amplitude. Interestingly, the monopole term in Equation (10) resolves the Hubble tension (Tiwari *et al.* 2022). For that, we need to choose the phase $\omega \neq \pi$. The range of parameters which explain both the matter dipole and the Hubble tension are given in Tiwari *et al.* (2022). In Table 2, we quote some of those values.

The superhorizon modes are also likely to leave their signatures in other cosmological observables like Baryon Acoustic Oscillations, epoch of reionziation, etc.

4. Constraints using SKA

4.1 *Superhorizon perturbation observation*

The superhorizon model predicts several observations, which can be tested with SKA and other future surveys. An interesting feature is the significant dependence of dipole on the redshift in the presence of superhorizon modes. Hence, the dipole measurements in redshift bins with SKA1 and SKA2 continuum survey can work as a potential test of the model. For a radio continuum survey, it is unlikely that we would have spectroscopic redshift information. In the past, redshifts of radio galaxies have been estimated by taking cross correlation with well known redshift surveys (Blake & Wall 2002; Tiwari *et al.* 2015). Such strategies are still viable by using data from the GAMA survey fields (Baldry *et al.*
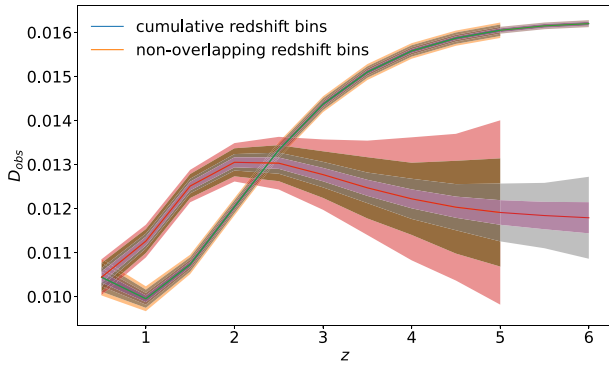
Figure 2. The dipole signal observation in the presence of superhorizon modes with SKA1 ($z \leq 5$) and SKA2 ($z \leq 6$) continuum surveys. The inner and outer shaded regions, respectively, represent the optimistic and realistic uncertainties for both SKA1 and SKA2. Here, we have assumed a superhorizon mode (Tiwari *et al.* 2022) satisfying the present NVSS dipole observation (Tiwari *et al.* 2015).

2018). However, new techniques like template fitting (Duncan *et al.* 2018) or machine learning-based photometric redshift computations (Brescia *et al.* 2021) make it possible for the SKA radio continuum survey galaxies to contain redshift information. This added information provides a unique possibility to test superhorizon mode physics with the SKA.

4.2 *Predictions*

Here, we demonstrate how precisely evident the dipole predictions with a superhorizon model would be. Further, we demonstrate how much they are constrained using SKA observations. Assuming superhorizon modes that (a) satisfy the present NVSS and Hubble parameter measurements and (b) are consistent with CMB and other cosmological measurements (see Table 2); we obtain the dipole magnitude $D_{\rm obs}$ in redshift bins using the formalism described in Tiwari *et al.* (2022). The dependence of dipole signal on the redshift z is shown in Figure 2, where we have shown the redshift dependence of $D_{\rm obs}$ for two cases

1. Cumulative redshift bins: For this case, we fix $z_1 = 0$ in Equation (7) and vary $z_2 = z$. In other words, we calculate $D_{\rm obs}(0, z)$.
2. Non-overlapping redshift bins: In this case, we obtain the non-overlapping z dependence by evaluating $D_{\rm obs}(z - \Delta z, z + \Delta z)$ with $\Delta z = 0.25$. For a fix Δz, this thus gives $D_{\rm obs}$ at z.

Table 3. Optimistic and realistic flux densities (in μJy) for SKA1 and SKA2 surveys

Flux density	SKA1	SKA2
Optimistic	>10	>1
Realistic	>20	>5

4.3 *Estimating uncertainties*

We employ (Alonso *et al.* 2015) 'Ultra-large scales' codes[2] (for continuum surveys) to determine the number densities for SKA surveys. We further assume that SKA1 and SKA2 will observe the sky up to respective declinations of 15° and 30°. The optimistic and realistic flux densities' limits for SKA1 and SKA2 (Bengaly *et al.* 2018; Square Kilometre Array Cosmology Science Working Group *et al.* 2020) are given in Table 3.

Additionally, we note that SKA1 is expected to probe up to $0 \leq z \leq 5$, whereas the SKA2 will reach up to redshift 6. We mock SKA1 and SKA2 continuum sky to determine the observational implications of the superhorizon model. We produce 1000 number density simulation of SKA1 and SKA2 continuum survey for each (optimistic and realistic) flux threshold using HEALPIX software (Goŕski*et al.* 2005), with $N_{\rm side} = 64$. The mean number of galaxies in a pixel is determined using number density obtained from Alonso *et al.* (2015) code and by modeling a dipole with magnitude and direction expected in presence of a superhorizon mode. Given the mean number density in a pixel, we call random Poisson distribution to emulate the galaxy count in the pixel. The galaxy mock thus neglects the cosmological galaxy clustering. This is justified since the clustering dipole in LSS is $\approx 2.7 \times 10^{-3}$ (Nusser & Tiwari 2015; Tiwari & Nusser 2016), which is roughly five times less than the apparent dipole in LSS[3] and inconsequential for our simulations. This is roughly equal to the uncertainties in the measured dipole is LSS using NVSS galaxies (Table 1). We consider SKA1, SKA2 sky coverage, i.e., mask declination above 15° and 30°, respectively. Additionally, we mask the galactic latitudes ($|b| < 10°$) to remove Milky Way contamination. The galactic plane cut is often chosen to be anywhere between $|b| < 5°$ and $|b| < 15°$, and in most studies, one tests the robustness of the results with varying redshift cuts.

---

[2]http://yintensitymapping.physics.ox.ac.uk/codes.html.

[3]These estimates correspond to NVSS galaxies. Assuming the NVSS measured dipole in LSS is true, we expect similar numbers from SKA continuum surveys.

For tests on mock data, here we choose a typical cut of $|b| < 10°$ that should balance the exclusion of galactic plane contamination and loss of sky fraction. Next, we use `Python Healpy`[4] (Górski *et al.* 2005; Zonca *et al.* 2019) `fit_dipole` function and obtain dipole for each 1000 mock maps. From these 1000 dipole values, we calculate the standard deviation to determine the uncertainty in measurements. The shaded regions in Figure 2 show the results obtained for SKA1 and SKA2 optimistic and realistic number densities in non-overlapping and cumulative redshift bins.

4.4 *Other anisotropy tests with SKA*

If the universe does not follow CP at large distance scales, then every observable should have directional dependence characteristics. Out of all, three observables are of particular interest as these are independent of the number density over the sky. So these are more robust under unequal coverage and systematics of the sky. These observables are

- Mean spectral index ($\bar{\alpha}$): As we said in Section 2.1.1, the spectral index for a radio source is defined between flux density and frequency through $S \propto \nu^{-\alpha}$. In the `Healpy` pixelation scheme, the sky is divided into equal area pixels. For a given pixel p with N_p sources having spectral indices $\alpha_{i,p}$, we define mean spectral index:

$$\bar{\alpha}_p = \frac{1}{N_p} \sum_i \alpha_{i,p}, \tag{11}$$

  here, i runs over all the sources in pixel p.
- Exponent (x) of differential number count: Defined using $N(S, \hat{\mathbf{n}}) \propto S^{-1-x}$.
- Average flux density ($\bar{S}$): We define this quantity for a pixel p:

$$\bar{S}_p = \frac{1}{N_p} \sum_i S_{i,p}, \tag{12}$$

  where again i runs over all the sources in p and N_p is the number of sources in the pixel.

The spectral index characterizes the morphology of an astronomical source. Angular dependence of $\bar{\alpha}$ has been moderately considered in the literature. Analysing the dipole anisotropy in $\bar{\alpha}$ has been a challenge, since it requires reliable multi-frequency continuum radio sky survey. Such an SKA survey can be used to estimate this

anisotropy if the flux density of the sources at different frequencies is measured with sufficient accuracy. For x, the angular dependency was analysed by Ghosh & Jain (2017) in NVSS data using likelihood maximization and the results were found to be consistent with CP. However, with a larger expected source count of SKA, i.e., almost twice in comparison to NVSS, angular dependence analysis of x may provide a more stringent test of CP.

SKA will also be able to test the phenomenon of alignment of radio galaxy axes and integrated polarizations, as claimed in earlier radio observations (Tiwari & Jain 2013, 2016; Taylor & Jagannathan 2016).

5. Conclusion and outlook

In this paper, we have reviewed several cosmological signals, which appear to show a violation of CP. We have also reviewed a model, based on aligned superhorizon modes, which can explain some of these observations along with the Hubble tension (Tiwari *et al.* 2022). The model can be theoretically justified by postulating a pre-inflationary phase during which the Universe may not be homogeneous and isotropic (Rath *et al.* 2013). The model leads to several cosmological predictions which can be tested at SKA. By using the best fit parameters with current observations, we have determined the redshift dependence of the predicted dipole in radio galaxy number counts and associated uncertainties. As can be seen from Figure 2, SKA can test this very reliably. If this prediction is confirmed by SKA, it may provide us with a first glimpse into the physics of the pre-inflationary phase of the Universe.

We have also suggested other isotropy tests with SKA using other variables, which are independent of number density and thus, are more robust under unequal coverage and systematics of the sky. These variables are (a) mean spectral index $\bar{\alpha}$, (b) exponent of the differential number count x and (c) average flux density $\bar{S}$.

---

[4]https://healpy.readthedocs.io/en/latest/index.html.

References

Alonso D., Bull P., Ferreira P. G., Maartens R., Santos M. 2015, ApJ, 814, 145

Aluri P. K., Jain P. 2012, Mod. Phys. Lett. A, 27, 50014

Aluri P. K., *et al.* 2022, arxiv:2207.05765

Anchordoqui L. A., Perez Bergliaffa S. E. 2019, Phys. Rev. D, 100, 123525

Baldry I. K., Liske J., Brown M. J. I., *et al.* 2018, MNRAS, 474, 3875

Bengaly C. A. P., Maartens R., Santos M. G. 2018, JCAP, 1804, 031

Blake C., Wall J. 2002, Nature, 416, 150

Bonvin C., Durrer R. 2011, Phys. Rev. D, 84, https://doi.org/10.1103/physrevd.84.063505

Brescia M., Cavuoti S., Razim O., *et al.* 2021, Front. Astron. Space Sci., 8, 70

Challinor A., Lewis A. 2011, Phys. Rev. D, 84, https://doi.org/10.1103/physrevd.84.043516

Coles P., Lucchin F. 2003, Cosmology: The Origin and Evolution of Cosmic Structure (New York: Wiley)

Colin J., Mohayaee R., Rameez M., Sarkar S. 2017, MNRAS, 471, 1045

Das K. K., Sankharva K., Jain P. 2021, JCAP, 2021, 035

de Oliveira-Costa A., Tegmark M., Zaldarriaga M., Hamilton A. 2004, Phys. Rev. D, 69, 063516

Domènech G., Mohayaee R., Patil S. P., Sarkar S. 2022, JCAP, 10, 019

Duncan K. J., Brown M. J. I., Williams W. L., *et al.* 2018, MNRAS, 473, 2655

Dunkley J., *et al.* 2011, ApJ, 739, 52

Einstein A. 1917, Sitzungsberichte der Koniglich Preusischen Akademie der Wissenschaften, Berlin, p. 172

Ellis G. F. R., Baldwin J. E. 1984, MNRAS, 206, 377

Ellis G. F. R., Maartens R., MacCallum M. A. H. 2012, Relativistic Cosmology, Cambridge University Press, Cambridge, https://doi.org/10.1017/CBO9781139014403

Erickcek A. L., Carroll S. M., Kamionkowski M. 2008a, Phys. Rev. D, 78, 083012

Erickcek A. L., Kamionkowski M., Carroll S. M. 2008b, Phys. Rev. D, 78, 123520

Flanagan E. E. 2005, Phys. Rev. D, 71, 103521

Freedman W. L., Madore B. F., Scowcroft V., *et al.* 2012, ApJ, 758, 24

Freedman W. L., Madore B. F., Gibson B. K., *et al.* 2001, ApJ, 553, 47

Gao X. 2011, Phys. Lett. B, 702, 12

Gayathri V., Healy J., Lange J., *et al.* 2020, 2009.14247

Ghosh S. 2014, Phys. Rev. D, 89, 063518

Ghosh S., Jain P. 2017, ApJ, 843, 13

Ghosh S., Jain P., Kashyap G., *et al.* 2016, JoAA, 37, 1

Gibelyou C., Huterer D. 2012, MNRAS, 427, 1994

Gordon C., Hu W., Huterer D., Crawford T. 2005, Phys. Rev. D, 72, 103002

Gordon C., Hu W., Huterer D., Crawford T. M. 2005, Phys. Rev. D, 72, 103002

Gor´ski K., Hivon E., Banday A., *et al.* 2005, ApJ, 622, 759

Grishchuk L. P., Zeldovich I. B. 1978a, AZh, 55, 209, [Sov. Astron. 22, 125 (1978)]

Grishchuk L. P., Zeldovich I. B. 1978b, Soviet Ast., 22, 125

Henning J. W., *et al.* 2018, ApJ, 852, 97

Hirata C. M., Seljak U. 2005, Phys. Rev. D, 72, 083501

Hoftuft J., Eriksen H. K., Banday A. J., *et al.* 2009, ApJ, 699, 985

Hutsemékers D. 1998, A&A, 332, 410

Jain P., Ralston J. P. 1999, MPLA, 14, 417

Jensen L. G., Stein-Schabes J. A. 1986, in International School of Particle Astrophysics: Gauge Theory and the Early Universe 0343

Kim Y., Park C.-G., Noh H., Hwang J.-C. 2021, arxiv:2112.04134

Kolb E., Turner M. 1994, The Early Universe, Frontiers in Physics, Westview Press

Krishnan C., Mohayaee R., Colgáin E. O., Sheikh-Jabbari M. M., Yin L. 2021, Class. Quant. Grav., 38, 184001

Mukherjee S., Ghosh A., Graham M. J., *et al.* 2020, 2009.14199

Nadolny T., Durrer R., Kunz M., Padmanabhan H. 2021, JCAP, 2021, 009

Nusser A., Tiwari P. 2015, ApJ 812, 85

Perivolaropoulos L., Skara F. 2022, New Astron. Rev., 95, arxiv:2105.05208

Planck Collaboration, Aghanim N., Armitage-Caplan C., *et al.* 2014, A&A, 571, A27

Planck Collaboration, Aghanim N., Akrami Y., *et al.* 2018, arxiv:1807.06209

Planck Collaboration, Aghanim N., Akrami Y., *et al.* 2020, A&A, 641, A6

Ralston J. P., Jain P. 2004, IJMPD, 13, 1857

Rath P., Mudholkar T., Jain P., Aluri P., Panda S. 2013, JCAP, 4, 7

Reid M. J., Pesce D. W., Riess A. G. 2019, ApJ, 886, L27

Riess A. G., Casertano S., Yuan W., Macri L. M., Scolnic D. 2019, ApJ, 876, 85

Rubart M., Schwarz D. J. 2013, A&A, 555, arxiv:1301.5559

Sato K. 1988, Symp. Int. Astron. Union, 130, 67

Secrest N. J., Hausegger S. V., Rameez M., *et al.* 2021, ApJ, 908, L51

Singal A. K. 2011, ApJL, 742, L23

Square Kilometre Array Cosmology Science Working Group, Bacon D. J., Battye R. A., *et al.* 2020, PASA, 37, e007

Stein-Schabes J. A. 1987, Phys. Rev. D, 35, 2345

Taylor A. R., Jagannathan P. 2016, MNRAS, 459, L36

Tiwari P., Jain P. 2013, Int. J. Mod. Phys. D, 22, 1350089

Tiwari P., Jain P. 2015, MNRAS, 447, 2658

Tiwari P., Jain P. 2016, MNRAS, 460, 2698

Tiwari P., Kothari R., Jain P. 2022, Astrophys. J. Lett., 924, L36

Tiwari P., Kothari R., Naskar A., Nadkarni-Ghosh S., Jain P. 2015, Astropart. Phys., 61, 1

Tiwari P., Nusser A. 2016, JCAP, 2016, 062

Wald R. M. 1983, Phys. Rev. D, 28, 2118R

Weinberg S. 1972, Gravitation and Cosmology: Principles and Applications of the General Theory of Relativity (New York: Wiley)

Wong K. C., Suyu S. H., Chen G. C. F., *et al.* 2020, MNRAS, 498, 1420

Zonca A., Singer L., Lenz D., *et al.* 2019, J. Open Source Softw., 4, 1298